Supplement of Atmos. Chem. Phys., 21, 4869–4897, 2021
https://doi.org/10.5194/acp-21-4869-2021-supplement

Supplement of

The impact of cloudiness and cloud type on the atmospheric heating rate of black and brown carbon in the Po Valley

Luca Ferrero et al.

Correspondence to: Luca Ferrero (luca.ferrero@unimib.it)

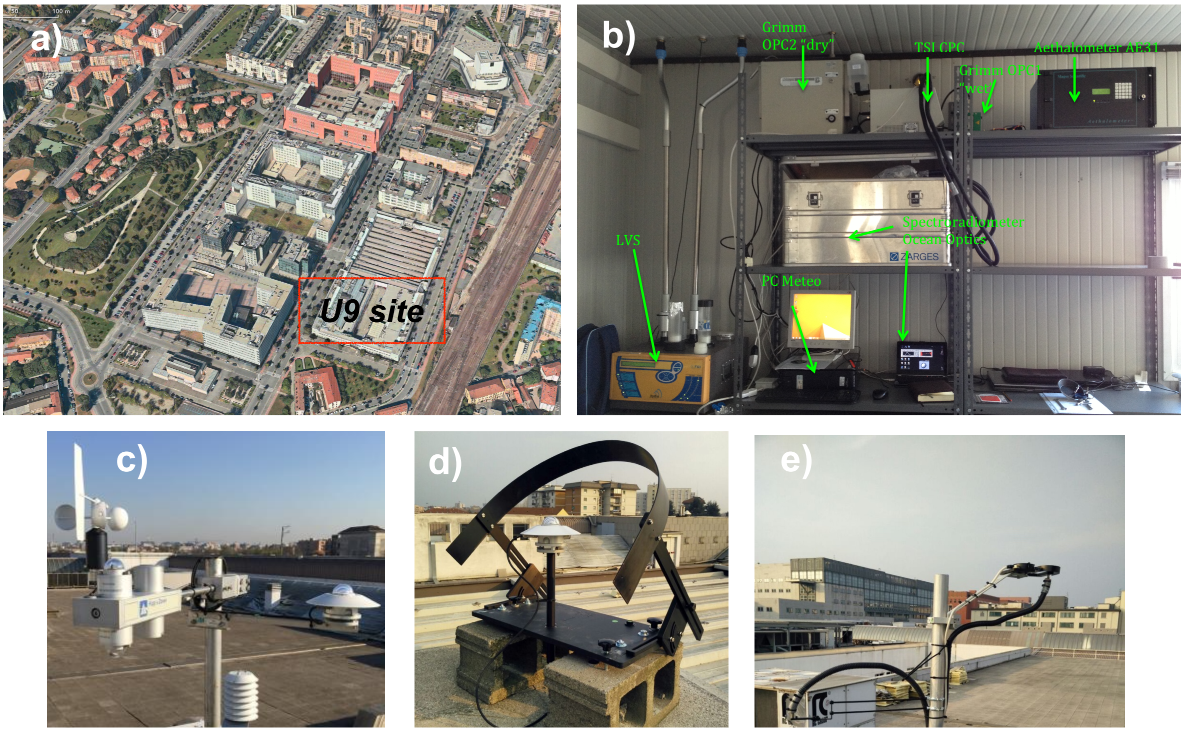

Figure S1. a) location of the U9 sampling site at the University of Milano-Bicocca; b) inner view of the site and of the instrumentation present there; c) Kipp&Zonen and LSI-Lastem radiometers (global, reflected), thermo-hygrometer and anemometer; d) LSI-Lastem radiometer and shadow-band for diffuse radiation; e) MRI (Multiplexer-Radiometer-Irradiometer) with rotating shadow-band. The copyright holder of panel a) is GoogleMaps (©GoogleMaps).

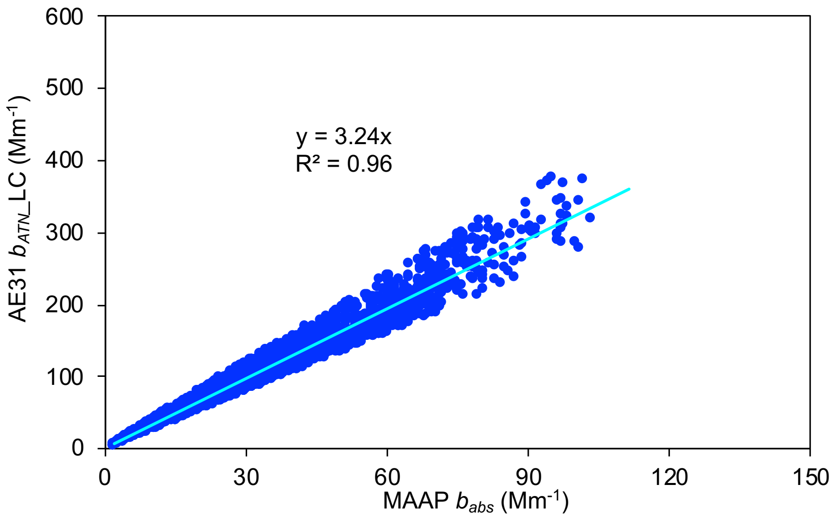

Figure S2. Linear correlation between the attenuation coefficient at 660 nm, yet loading corrected ($b_{ATN\_LC,660nm}$ following Weingartner et al., 2003; section 2.2) from the AE31 Aethalometer and the MAAP absorption coefficient at the same wavelength.

Measured and computed C factor

To verify the reliability of the obtained *C* value, it was also computed following the Collaud Coen et al. (2010) procedure. They defined the reference value of *C* (C_{ref} = 2.81±0.11) for the AE31 tape based on data from pristine environments (Jungfraujoch and Hohenpeissenberg sites where aerosol has a single scattering albedo of ~1); at the same time, Collaud Coen et al. (2010) defined *C* for any kind of aerosol as follows:

$$C = C_{ref} + \alpha \frac{\omega_0}{1-\omega_0} \quad \text{(S1)}$$

where α is the parameter for the Arnott (2005) scattering correction (0.0713 at 660 nm) and ω_0 the single scattering albedo. In wintertime in Milan, within the mixing layer, the single scattering albedo was found to be 0.846±0.011 at 675 nm by Ferrero et al. (2014). From eq. 1 it follows that the expected *C* in Milan is 3.20±0.35; within its range the experimental 3.24±0.03 value lies. With respect to *C* interpretation, we need to underline first that the nominal AE31 660 nm channel is provided by a Kingbright light-emitting diode (APT 1608SRC PRV 1.6 x 0.8 mm SMD Chip LED Lamp; King bright, 2018) which is characterized by a 20 nm spectral full bandwidth at half maximum under 20mA of supplied current (information from manufacturer). This is in agreement with the absorption photometer intercomparison, reported by Müller et al. (2011), in which the nominal AEs red channel was found to have a 23 nm spectral full bandwidth at half maximum. Thus, for practical purposes, the single scattering albedo (0.846±0.011 at 675 nm) reported in Milan at a wavelength slightly different from the one featured in the AE31 by Ferrero et al. (2014) was applied to eq. S1.

Physical meaning of HR equation (linkage with the actinic flux)

Equation 2 in the main body of the manuscript implies that the calculation of the HR requires the summatory of the total amount of radiative energy interacting with LAA, thus also including the reflected radiance other than the diffuse one and the direct component from the sun. In fact an alternative writing of equations 2 is:

$$HR = \frac{1}{\rho C_p} \cdot \int_{\lambda=300}^{\lambda=3000} AF(\lambda) b_{abs(\lambda)} d\lambda \quad \text{(S2)}$$

where AF(λ) represents the actinic flux, that is the total spectral flux of photons per unit area and wavelength interval available to molecules/aerosol at a particular point in the atmosphere. The radiative flux from all directions onto a volume of air is called the actinic flux (Seinfeld and Pandis, 2006).

The actinic flux consists of three components: direct solar radiation, diffuse radiation originating from scattering in the atmosphere, and diffuse radiation originating from reflection from the Earth's surface.

Thus, for the AF the following sum is valid:

$$AF_{tot} = AF_{dir} + AF_{dif} + AF_{ref} \quad \text{(S3)}$$

The actinic flux at a particular point in the atmosphere is calculated by integrating the spectral radiance over all directions of space. The actinic flux must be distinguished from spectral irradiance, which is the hemispherically integrated radiance weighted by the cosine of the angle of incidence, and represents the photon flux per unit area through a plane surface. Under the isotropic and Lambertian assumptions, the diffuse and reflected irradiances are related with the corresponding radiances by a factor π; the direct irradiance is related to the radiance as a function of the solar zenith angle (θ_z).

From a physical point, given a generic monochromatic radiance R(λ,θ,ϕ) (in function of wavelength, zenith and azimuth), the corresponding AF(λ) and irradiance F(λ) (Seinfeld and Pandis, 2006; Liou, 2007) are given by:

$$AF(\lambda) = \int_{\phi=0}^{\phi=2\pi} \int_{\theta=0}^{\theta=\pi/2} R(\lambda,\theta,\phi) \sin(\theta)\, d\theta d\phi \quad \text{(S4)}$$

$$F(\lambda) = \int_{\phi=0}^{\phi=2\pi} \int_{\theta=0}^{\theta=\pi/2} R(\lambda,\theta,\phi) \cos(\theta) \sin(\theta)\, d\theta d\phi \quad \text{(S5)}$$

For the direct component, the radiance comes only from the sun direction (the solar zenith angle, θ_z), it can be assumed to be a collimated beam, essentially parallel, and originates from a very small solid angle and thus:

$$AF_{dir}(\lambda) = R_{dir}(\lambda) = F_{dir}(\lambda)/\cos(\theta_z) \tag{S6}$$

For the diffuse and reflected component (under the isotropic and Lambertian assumptions, respectively) the radiance comes homogeneously from each direction and thus:

$$AF_{dif,ref}(\lambda) = 2\pi R_{dif,ref}(\lambda) \tag{S7}$$

$$F_{dif,ref}(\lambda) = \pi R_{dif,ref}(\lambda) \tag{S8}$$

implying:

$$AF_{dif,ref}(\lambda) = 2F_{dif,ref}(\lambda) \tag{S9}$$

Now, as in section 2.2 we gave the following definition:

$$HR = HR_{dir} + HR_{dif} + HR_{ref} \tag{S10}$$

we can finally rewrite it (given eq. A7 and A8) as follows:

$$HR = \frac{1}{\rho C_p} \cdot \left[\frac{1}{\cos(\theta z)} \int_\lambda F_{dir}(\lambda)\, b_{abs}(\lambda)\, d\lambda + 2\int_\lambda F_{dif}(\lambda)\, b_{abs}(\lambda)\, d\lambda + 2\int_\lambda F_{ref}(\lambda)\, b_{abs}(\lambda)\, d\lambda\right] \tag{S11}$$

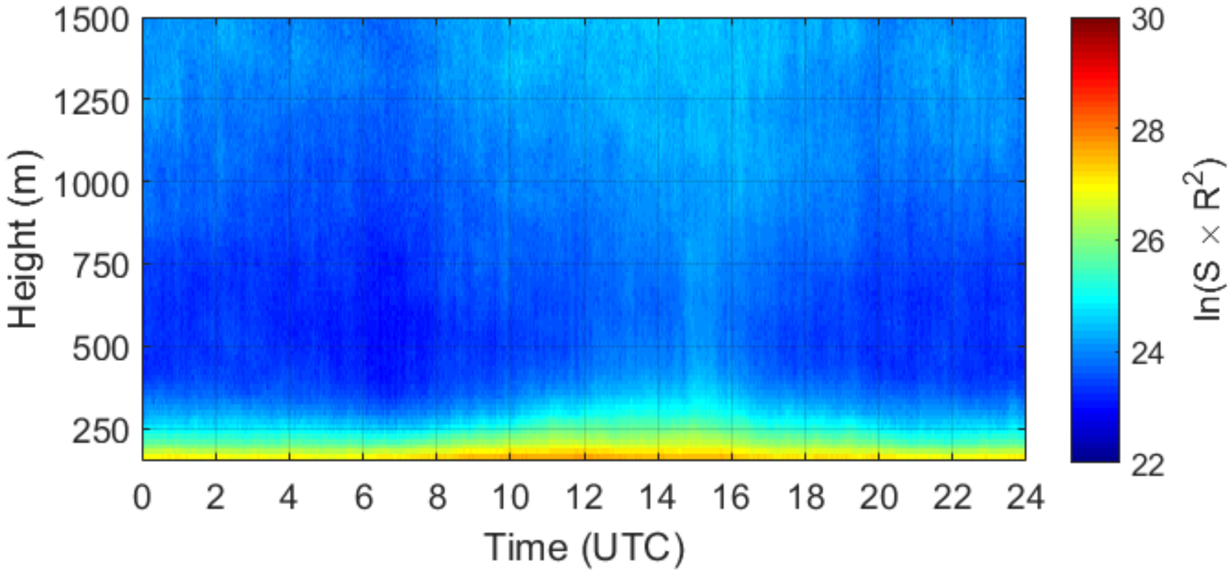

Figure S3. Milan averaged wintertime lidar range corrected signal during the campaign presented in the manuscript.

N	0	1	2	3	4	5	6	7	8
a_0	-112.6	-112.6	-107.3	-97.8	-85.1	-77.1	-71.2	-31.8	-13.7
a_1	653.2	686.5	650.2	608.3	552.0	511.5	495.4	287.5	154.2
a_3	174.0	120.9	127.1	110.6	106.3	58.5	-37.9	94.0	64.9
a	0.73	0.72	0.72	0.72	0.72	0.70	0.70	0.69	0.69
L	-95.0	-89.2	-78.2	-67.4	-57.1	-45.7	-33.2	-16.5	-4.3

Table S1. The empirical coefficients relating the global radiation, at a fixed solar elevation angle ($\pi/2-\theta$), with the sky conditions (N, in oktas) extracted from the original work of Ehnberg and Bollen (2005).

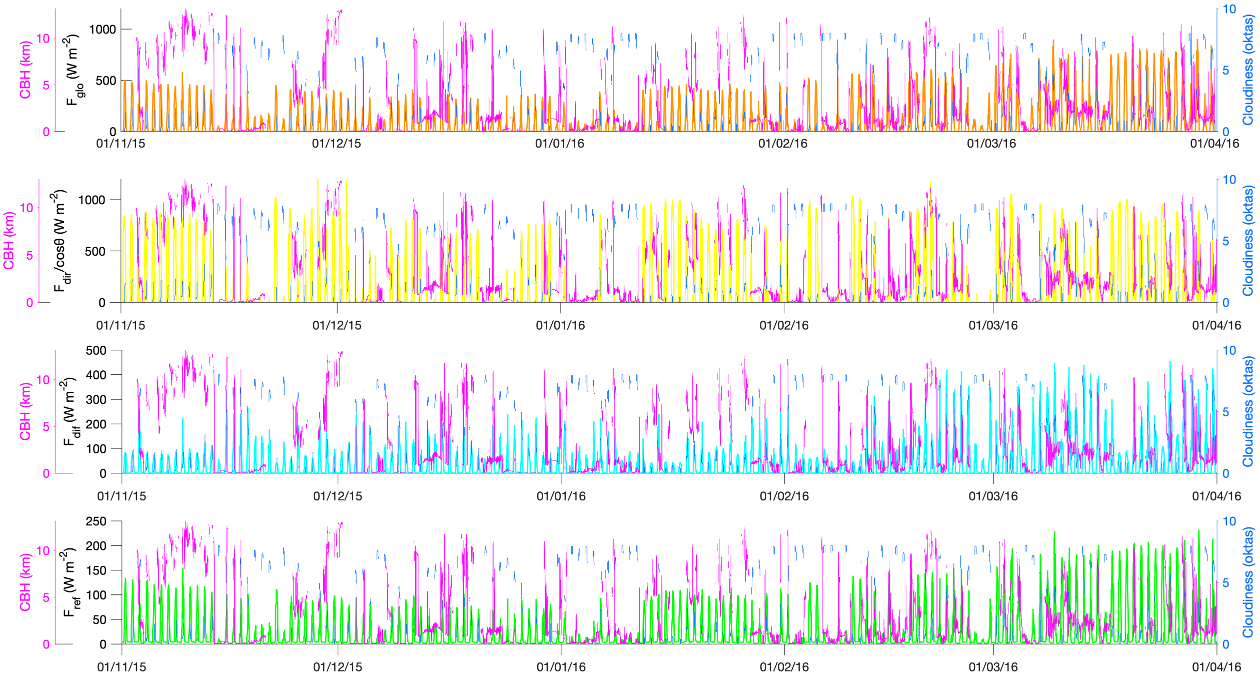

Figure S4. 5-min resolution data for the global radiation values (F_{glo}) and their direct, diffuse and reflected components ($F_{dir}/cos\,\theta_z$, F_{dif} and F_{ref}). Once F_{dir} is scaled by $cos\,\theta_z$ (eq. 1, section 2.1) it is quite constant along the year and it is perfectly constant only in clear sky conditions. Conversely, the diffuse and reflected radiation, even when scaled by $cos\,\theta$ (under the isotropic and Lambertian assumptions), linearly follow the behavior of irradiance F_{dif} and F_{ref} (see eq. S7 and S8).

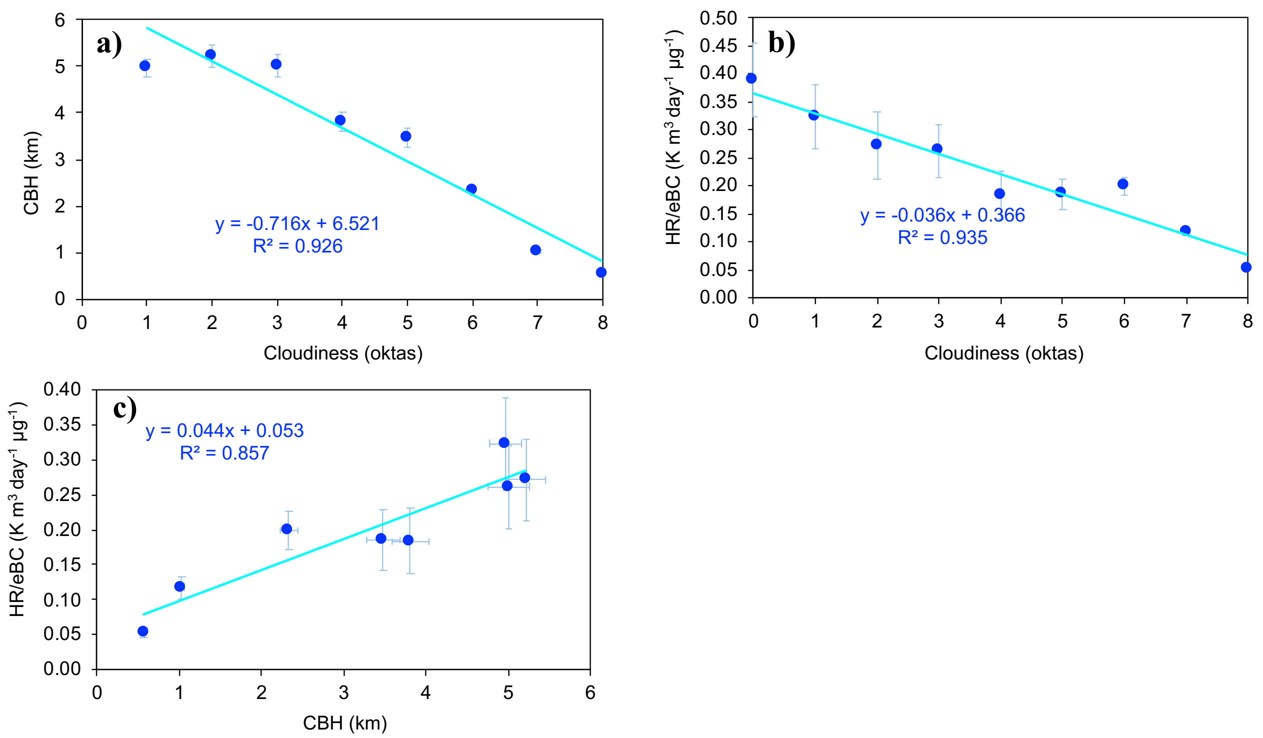

Figure S5. Relationship between cloud base height (CBH) and cloudiness (oktas) (a), HR/eBC and cloudiness (b) HR/eBC and CBH.

Wind speed, cloudiness and clouds

The cloudiness is a non-linear function of the cloud type, as cloud type are related to the meteorological patterns: e.g. highly persistent stratiform clouds generate cloudy weather in conditions with lower wind. A brief explanation could be given considering the wind speed in the 20 minute interval of the Duchon and O'Malley (1999) method (section 2.3.2). The SD changes in the global irradiance is due to the wind influence on the cloud dynamic; despite the fact that the wind influence on the aforementioned process is the wind at the clouds altitude, we investigated the ground level wind behavior for the clouds type classified in the present work. Result are reported in Figure S7 (Supplemental material). As expected there is no strong correlation between the two parameters as the wind speed was measured at ground level and reflect the stagnant conditions typical of the Po Valley. The average wind speed during each cloud type and CS condition was below 1 m s^{-1}. Despite this, it is clearly visible that low-level clouds (e.g. stratus) are present in the lowest wind speed conditions. Particularly, the average ground wind speed in stratus conditions was 0.64±0.02 m s^{-1}, lower than the 0.92±0.04-1.04±0.03 m s^{-1} found in cirrus-clear sky conditions.

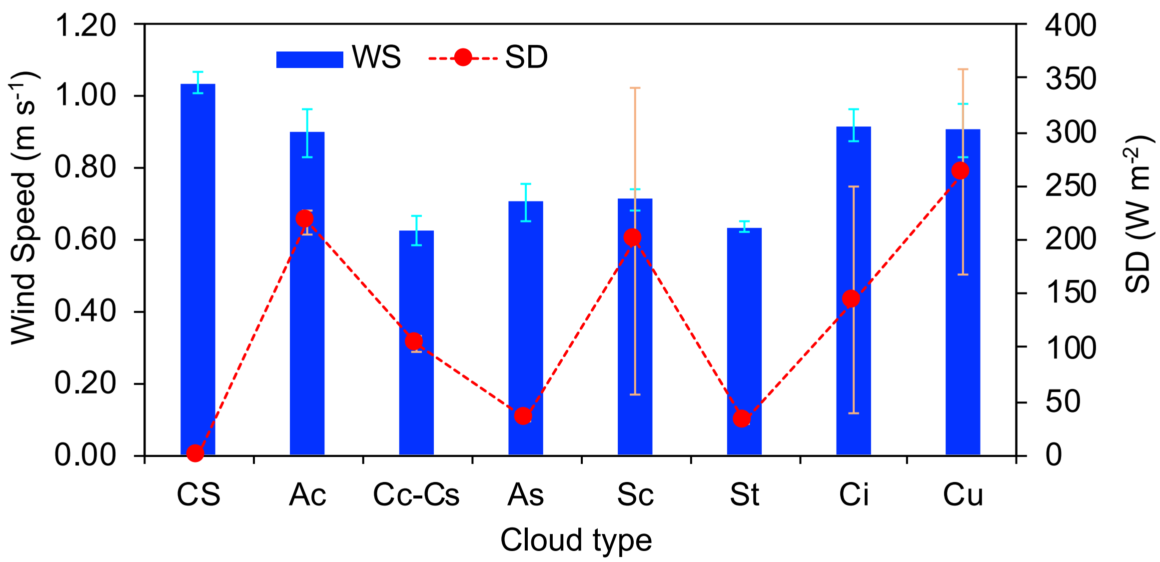

Figure S6. Wind speed (at ground) and SD for each cloud type.

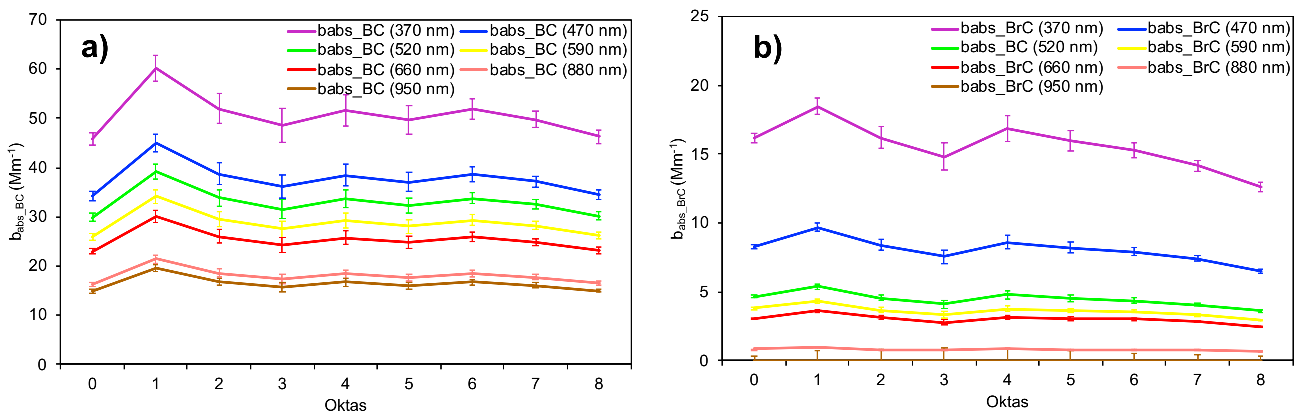

Figure S7. $b_{abs(\lambda)}$ values at the aethalometer 7-λ for both BC and BrC in function of the sky cloudiness expressed in oktas.

The role of average photon energy on the HR of BC and BrC

The HR_{BrC} values normalized to the species absorption coefficient in Figure 16 were always greater or equal to the corresponding normalized HR_{BC} for the same cloud type (even though the 95% confidence interval bands overlapped). A possible explanation can be found in the synergic effect of the different spectral absorption of BC and BrC and of the influence of clouds on the energy of the impinging radiation.

The average photon energy (APE) describes the spectral characteristics of direct, diffuse and reflected irradiance modulated by sky conditions with a single parameter. APE quantifies the spectral shape of irradiance and represents the average energy of photons impinging upon a target, in this case the aerosol layer close to the surface. Therefore, a single APE value can identify a unique spectral irradiance distribution which describes the light available for absorption in different spectral regions. APE was determined for each sky condition (and thus cloud type) from the measurements of the multiplexer-radiometer-irradiometer. APE (expressed in eV) was calculated dividing the total energy in a spectrum by the total number of photons it contains (Norton et al., 2015):

$$APE_{dir,dif,ref} = \frac{1}{q}\left[\frac{\int_{\lambda=350}^{\lambda=1000} F_{dir,dif,ref}(\lambda)d\lambda}{\int_{\lambda=350}^{\lambda=1000} \Phi_{\lambda} d\lambda}\right] \quad \text{(S12)}$$

where q represents the electron charge, $F_{dir,dif,ref}(\lambda)$ refers to the spectral direct, diffuse and reflected irradiance at wavelength λ (W m^{-2} nm^{-1}), and Φ_λ (number of photons m^{-2} s^{-1} nm^{-1}) is the photon flux density at wavelength λ determined using the Plank-Einstein equation:

$$\Phi_{\lambda} = \frac{F_{dir,dif,ref(\lambda)}}{hc/_{\lambda}} \quad \text{(S13)}$$

where h is the Plank constant and c the speed of light.

From eq. S12 it follows that APE is normalized for the total amount of irradiance, and therefore independent from the absolute intensity of light and indicating only the average distribution of light across the spectrum. Particularly, higher APE values describe the shift of a radiation spectrum towards the UV-blue region (Figure S8).

Characteristic APE values of direct (APE_{dir}), diffuse (APE_{diff}) and reflected (APE_{ref}) irradiance measured at the U9 site for different cloudiness are presented in Figure S9 and can explain why HR_{BrC} values in Figure 16 were always greater or equal to the corresponding ones of BC. This results from the combination of the different spectral absorption of BC and BrC and of the different influence of clouds on the direct, reflected and diffuse components of the spectral irradiances. As the BrC has the capacity to absorb much more radiation in the UV-blue region (featuring AAE of 3.49±0.01, compared to ~1 of BC) it follows that, depending on sky conditions BrC behavior can deviate from that of BC.

This can be related to the different APE of the direct, diffuse and reflected irradiance in different sky conditions. Figure S9 shows that while APE_{dir} and APE_{ref} slightly increases towards overcast conditions, APE_{dif} strongly decreased with cloudiness. The $APE_{dir,dif,ref}$ behavior can easily be explained (Figures S8 and S10): in clear sky conditions, the diffuse irradiance is characterized by a high density in the UV-blue high energy region with respect to the direct and reflected irradiance, which indeed are depleted in that region by the molecular Rayleigh scattering and the ground absorption, respectively. APE_{dir} and APE_{ref} in clear sky conditions were 1.89±0.01 and 1.87±0.01 eV, lower than the corresponding 2.20±0.01 eV of APE_{dif} (Figures S9-10). Conversely, in cloudy conditions (Figures S9-10) the cloud droplet scattering dominates and APE_{dif} values equaled that of APE_{dir}: 1.99±0.01 eV (APE_{ref} was 1.91±0.01 eV) being $F_{dif}(\lambda)$ and $F_{dir}(\lambda)$ similar (Figure S9).

As the BrC has the capacity to absorb much more radiation in the UV-blue region (featuring higher APE) it follows that, depending on sky conditions BrC can deviate from the BC behavior. In this respect, when APE for the total sky irradiance (APE_{tot}) was determined as a weighted average with respect to the absolute amount of direct, diffuse and reflected component (Figure S9) it showed an increasing APE_{tot} from CS to cloudy conditions, approaching APE_{dif} at okta=8. This

APE_{tot} feature explain the counter-intuitive property that cloudy conditions suppress slightly more the normalized HR_{BC} with respect to the normalized HR_{BrC}, as shown in Figure 16.

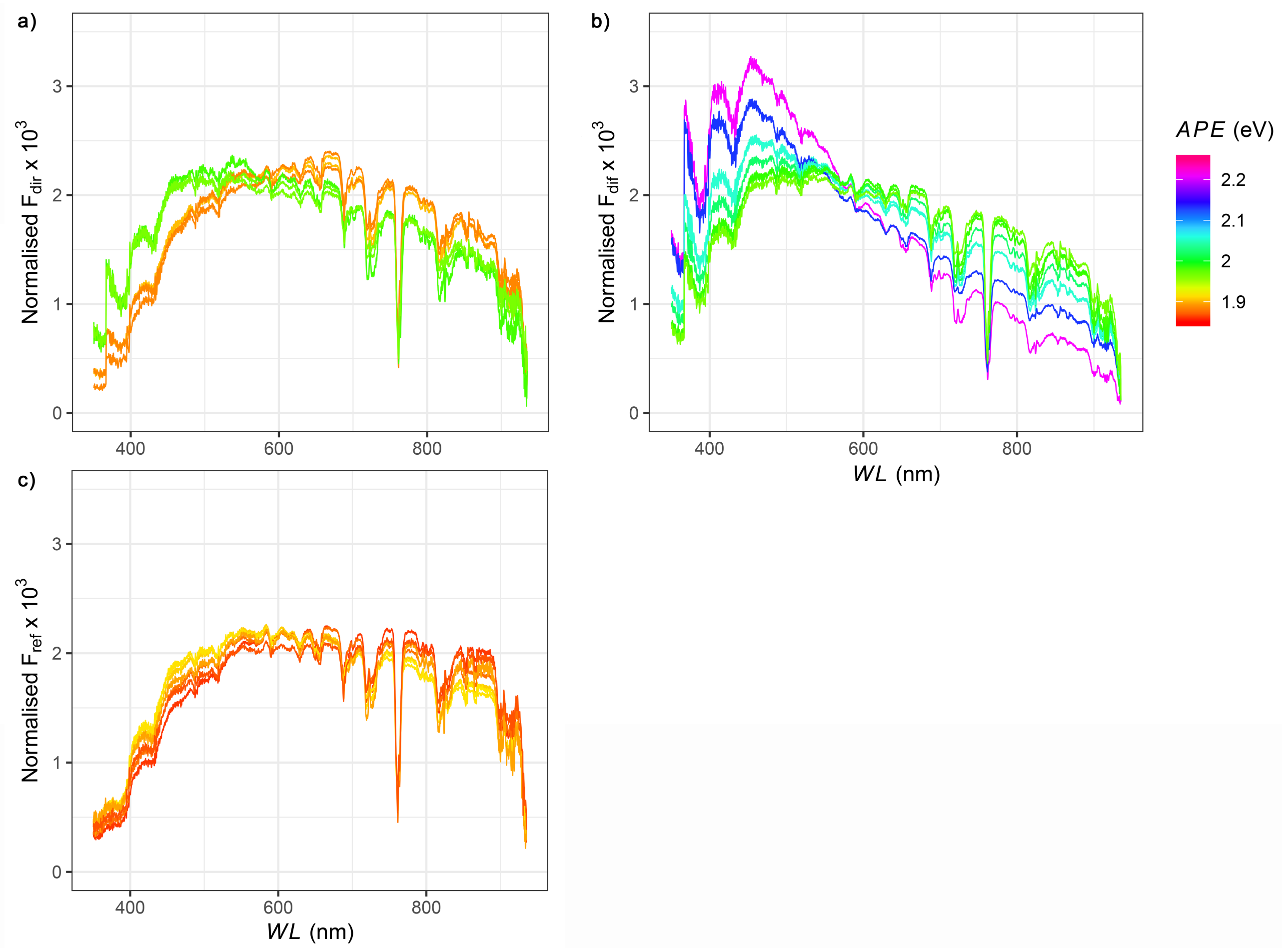

Figure S8. Average photon energy of different shape of radiation spectra for a) the direct and b) the diffuse and c) reflected irradiance .

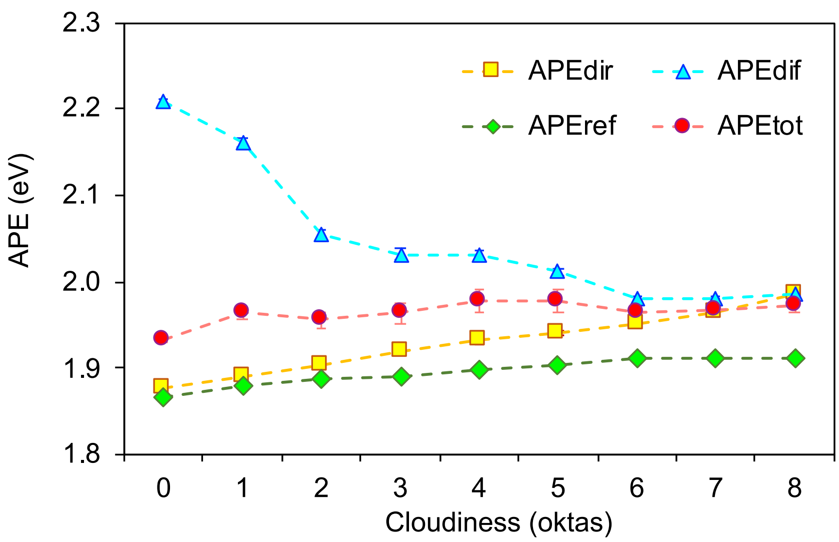

Figure S9. Direct, diffuse and reflected average photon energy of the radiation (APE_{dir}, APE_{dif} and APE_{ref}) together with the total one (APE_{tot}).

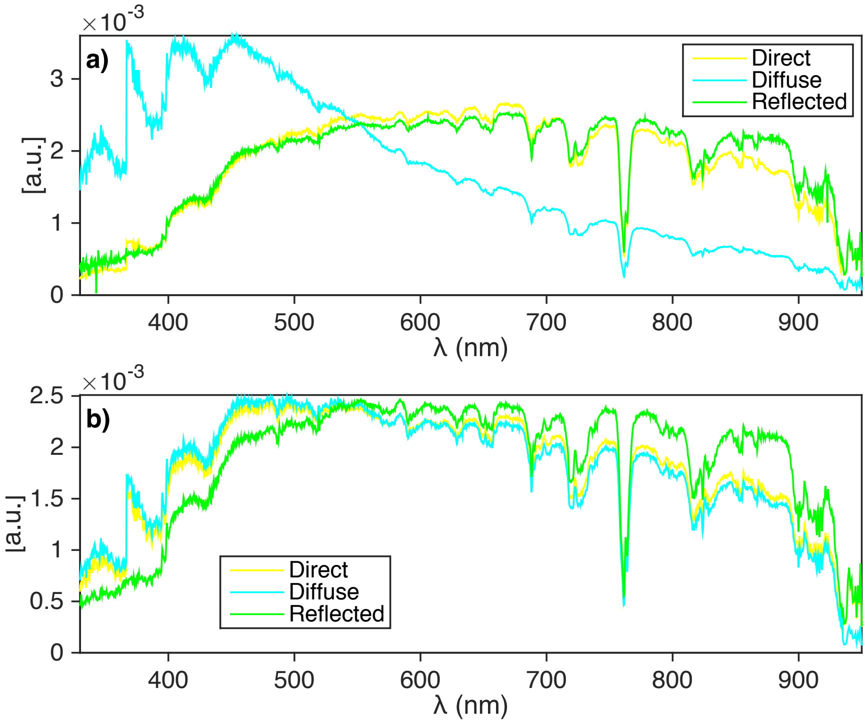

Figure S10. Normalized (integral equal to unity) spectra for direct (yellow), diffuse (ciano) and reflected (green) radiation in a clear sky (a) and in a cloudy (b) case.

References

Collaud Coen M., Weingartner E., Apituley A., Ceburnis D., Fierz-Schmidhauser R., Flentje H., Henzing J.S., Jennings S.G., Moerman M., Petzold A., Schmid O., and Baltensperger U. Minimizing light absorption measurement artifacts of the Aethalometer: evaluation of five correction algorithms. Atmos. Meas. Tech., 3, 457–474, 2010.

Duchon, C.E., O'Malley, M.: Estimating Cloud Type from Pyranometer Observations. J. App. Meteorology, 38, 132–141, 1999.

Ehnberg, J. S. G. and Bollen, M. H. J.: Simulation of global solar radiation based on cloud observations, Solar Energy, 78(2), 157–162, doi:10.1016/j.solener.2004.08.016, 2005.

Ferrero, L., Castelli, M., Ferrini, B.S., Moscatelli, M., Perrone, M.G., Sangiorgi, G., Rovelli, G., D'Angelo, L., Moroni, B., Scardazza, F., Mocnik, G., Bolzacchini, E., Petitta, M., Cappelletti, D.: Impact of Black Carbon Aerosol over Italian basin valleys: high resolution measurements along vertical profiles, radiative forcing and heating rate. Atmos. Chem. Phys., 14, 9641–9664, 2014.

Kingbright: APT1608SRCPRV, 1.6 x 0.8 mm SMD Chip LED Lamp - Specifications, [online] Available from: https://www.kingbrightusa.com/images/catalog/SPEC/APT1608SRCPRV.pdf, (last access: 11 November 2020), 2018.

Liou K.N.: An Introduction to Atmospheric Radiation, Second Edition. INTERNATIONAL GEOPHYSICS SERIES, Volume 84, Academic Press, 2007.

Müller, T., Henzing, J. S., de Leeuw, G., Wiedensohler, A., Alastuey, A., Angelov, H., Bizjak, M., Collaud Coen, M., Engström, J. E., Gruening, C., Hillamo, R., Hoffer, A., Imre, K., Ivanow, P., Jennings, G., Sun, J. Y., Kalivitis, N., Karlsson, H., Komppula, M., Laj, P., Li, S.-M., Lunder, C., Marinoni, A., Martins dos Santos, S., Moerman, M., Nowak, A., Ogren, J. A., Petzold, A., Pichon, J. M., Rodriquez, S., Sharma, S., Sheridan, P. J., Teinilä, K., Tuch, T., Viana, M., Virkkula, A., Weingartner, E., Wilhelm, R., and Wang, Y. Q.: Characterization and intercomparison of aerosol absorption

photometers: result of two intercomparison workshops, Atmos. Meas. Tech., 4, 245–268, https://doi.org/10.5194/amt-4-245-2011, 2011.
Norton, M., Amillo, A. M. G. and Galleano, R.: Comparison of solar spectral irradiance measurements using the average photon energy parameter, Solar Energy, 120, 337–344, doi:10.1016/j.solener.2015.06.023, 2015.
Seinfeld, J. H. and Pandis, S. N.: Atmospheric chemistry and physics – From air pollution to climate change, Wiley-Interscience, second edition, 2006.